Natural Resources Canada
Ressources naturelles Canada

Porosity reduction due to compaction versus texture variation effects in four compaction zones in the Beaufort-Mackenzie Basin, Northwest Territories

T.J. Katsube and S. Connell-Madore

Geological Survey of Canada
Current Research 2012-6

2012

Canada

Geological Survey of Canada
Current Research 2012-6

Porosity reduction due to compaction versus texture variation effects in four compaction zones in the Beaufort-Mackenzie Basin, Northwest Territories

T.J. Katsube and S. Connell-Madore

2012

ISSN 1701-4387
Catalogue No. M44-2012/6E-PDF
ISBN 978-1-100-20476-5
doi:10.4095/290225

A copy of this publication is also available for reference in depository libraries across Canada through access to the Depository Services Program's Web site at http://dsp-psd.pwgsc.gc.ca

A free digital download of this publication is available from GeoPub: http://geopub.nrcan.gc.ca/index_e.php

Toll-free (Canada and U.S.A.): 1-888-252-4301

Recommended citation

Katsube, T.J. and Connell-Madore, S., 2012. Porosity reduction due to compaction versus texture variation effects in four compaction zones in the Beaufort-Mackenzie Basin, Northwest Territories; Geological Survey of Canada, Current Research 2012-6, 12 p. doi:10.4095/290225

Critical review
B. Medioli

Authors
T.J. Katsube (John.Katsube@NRCan-RNCan.gc.ca)
S. Connell-Madore (Shauna.Connell-Madore@NRCan-RNCan.gc.ca)
Geological Survey of Canada
601 Booth Street
Ottawa, Ontario
K1A 0E8

Correction date:

Porosity reduction due to compaction versus texture variation effects in four compaction zones in the Beaufort-Mackenzie Basin, Northwest Territories

T.J. Katsube and S. Connell-Madore

Katsube, T.J. and Connell-Madore, S., 2012. Porosity reduction due to compaction versus texture variation effects in four compaction zones in the Beaufort-Mackenzie Basin, Northwest Territories; Geological Survey of Canada, Current Research 2012-6, 12 p. doi:10.4095/290225

Abstract: Porosity values for 41 shale samples were previously collected from nine petroleum exploration wells in four varied compaction zones in the Beaufort-Mackenzie Basin. These values generally showed a decrease with increased depth, as expected. But they also showed a general decrease as the sample locations moved from offshore toward the onshore locations of the basin. A shale-texture analysis was performed on 27 of these samples for the purpose of determining if these general porosity characteristic changes from offshore to onshore were influenced by shale-texture changes.

Results of this study have shown that while the shale-texture changes have shown some influence on the porosity characteristics, their influences were generally minor and often insignificant, and that compaction stress due to increased depth is the main influence on these porosity characteristics. Also, the sample porosity values showed a general decrease from offshore to onshore locations.

Résumé : Des valeurs de porosité ont été obtenues antérieurement pour 41 échantillons de shale recueillis dans neuf puits d'exploration pétrolière situés dans quatre zones de compaction différentes du bassin de Beaufort-Mackenzie. En général, ces valeurs diminuaient avec l'augmentation de la profondeur, comme on pouvait s'y attendre. Cependant, elles diminuaient également de façon générale à mesure que les sites d'échantillonnage migraient de la zone extracôtière à la zone continentale du bassin. Une analyse de la texture du shale a été effectuée sur 27 de ces échantillons dans le but de déterminer si ces changements généraux des caractéristiques de la porosité, qui accompagnent le passage de la zone extracôtière à la zone continentale, ont été influencés par des changements de texture du shale.

Les résultats de la présente étude ont démontré que, bien que les changements de texture du shale indiquent une certaine influence sur les caractéristiques de porosité, leur influence est généralement mineure et souvent négligeable, et que la contrainte due à la compaction liée à l'accroissement de la profondeur exerce la principale influence sur ces caractéristiques de porosité. Par ailleurs, les échantillons montrent une diminution générale de porosité en passant de la zone extracôtière à la zone continentale du bassin.

INTRODUCTION

With increased burial depth and compaction, shales evolve into effective seals that form barriers to the upward migration of fluids and gases, including CO_2 (Katsube et al., 2006). Therefore, compacted shales can act as caprocks for oil and gas accumulation and CO_2 sequestration and can contribute to the development of abnormal formation pressures (e.g. Huffman and Bowers, 2002) that can become a source of blowouts during drilling (e.g. Bowers, 1995). This is because the shale's sealing capacity increases as compaction reduces the number and size of the storage and connecting pores (Bowers and Katsube, 2002). Connecting porosity (ϕ_C) mainly contributes to fluid migration and storage porosity (ϕ_S) mainly contributes to fluid and gas storage. Effective porosity (ϕ_E) is the sum of these two porosities and is usually referred to as just porosity (ϕ).

Porosity was previously determined by downhole geophysical logs in nine petroleum exploration wells (Fig. 1; Issler, 1992) in four varied compaction zones (CZ) in the Beaufort-Mackenzie Basin, Northwest Territories, Northern Canada (Fig. 2; Issler et al., 2002). Porosity was later determined for 41 shale samples from these nine wells by laboratory methods (Issler and Katsube, 1994). All these

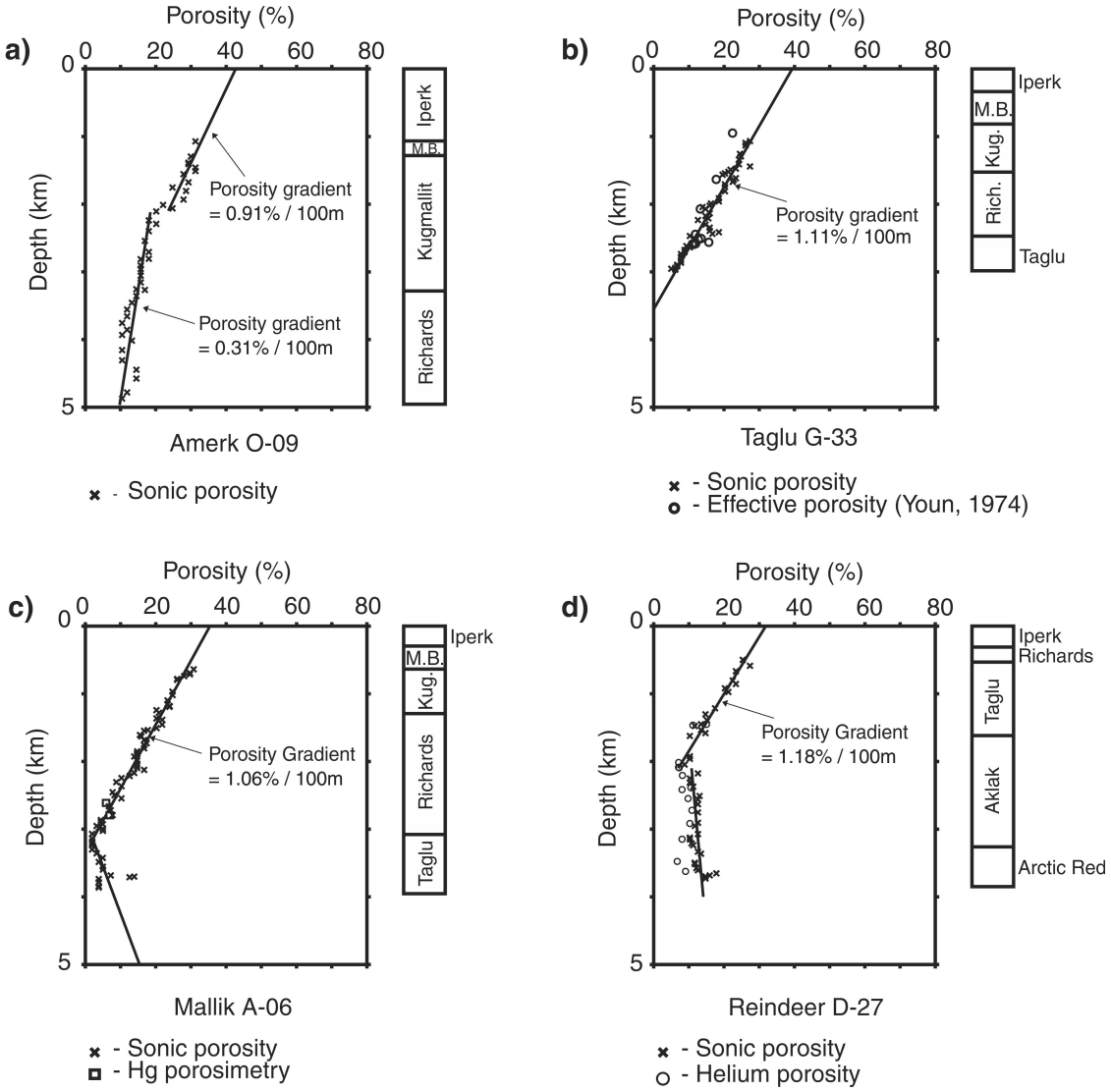

Figure 1. Examples of the sonic porosity (ϕ_G) (determined by using downhole sonic logs and the method of Issler (1992)) versus depth (h) relationship for four of the nine wells in four of the compaction zones (CZ) in the Beaufort-Mackenzie Basin. **a)** The ϕ_G-h relationship for well Amerk O-09 (CZ-2) represents the trend in CZ-1 and CZ-2. **b) and c)** The ϕ_G-h relationship for well Taglu G-33 (CZ-3) and Mallik A-06 (CZ-4), represents the trends in the northern section of CZ-4 and southern section of CZ-3. **d)** The ϕ_G-h relationship for well Raindeer D-27 (CZ-4), represents the trend in the southern section of CZ-4. Sequence names: M.B. – Mackenzie Bay; Kug, – (Kugmallit; Rich, - Richards: Hg porosity is from Katsube and Issler (1993) and helium porosity is from Issler and Katsube (1994).

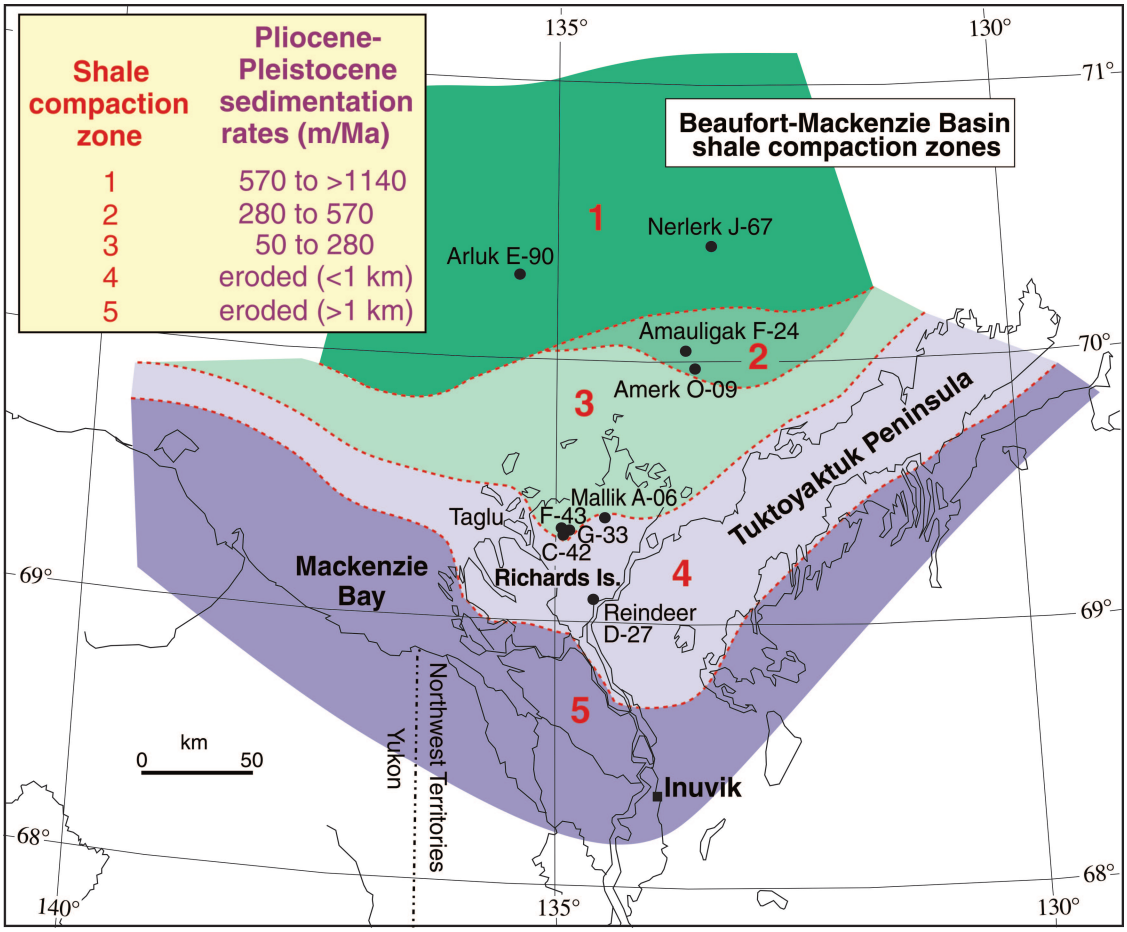

Figure 2. Locations of the nine petroleum exploration wells in the Beaufort-Mackenzie Basin, Northwest Territories, and the approximate boundaries of the five shale compaction zones (CZ) (Issler, 1992), which are shown in heavy dashed lines (from Issler et al., 2002). The numbers 1 to 5 represent the five compaction zones CZ-1 to CZ-5

porosity values decrease with increased depth at the initial stage of depth (2–4 km), as expected, but from about 2 to about 4 km depths they tended to level off or show a repetition of slight increases and decreases with depth, as shown in Figure 1.

It is interesting that all of these porosities for the initial stages of the porosity-versus-depth curves, both downhole and laboratory (e.g. Fig. 3a), tend to show a general decrease from offshore to onshore regions, regardless of the location of the exploration well they are from. The question is whether this trend is due to changes in compaction pressure from offshore to onshore, or whether there is a shale-texture change from offshore to onshore. In this study the shale texture has been examined for 27 of the 41 shale samples for the purpose of determining whether these general porosity changes from offshore to onshore are due to increased compaction pressure or due to shale-texture changes.

In a recent study (Katsube et al., 2011) all three porosities (ϕ_E, ϕ_S, ϕ_C) have shown a general decrease from offshore to onshore regions, as shown in Figure 3. These are significant parameters for characterizing seal quality and developing seal-quality evaluation methods, which are important for the efficiency and safety of petroleum and hydrocarbon gas exploration and for CO_2 sequestration. Therefore, it is essential to know the reason for this porosity decrease from offshore to onshore in the Beaufort-Mackenzie Basin.

SHALE COMPACTION ZONES

The 41 shale samples (Table 1) used for porosity measurements were previously collected from conventional cores of Cretaceous and Paleogene sediments below the Pliocene-Pleistocene formations over a depth range of approximately 950 to 4860 m in nine petroleum exploration wells (Katsube and Issler, 1993) in the Beaufort-Mackenzie Basin. These samples are from normally pressured and overpressured sediments in four of the five shale compaction zones (CZ) shown in Figure 2 (Issler et al., 2002). The lowest compaction zones are associated with the highest Pliocene-Pleistocene sedimentation rates and the highest compaction zones are associated with lowest Pliocene-Pleistocene sedimentation rates (Issler, 1992). CZ-1 is the compaction

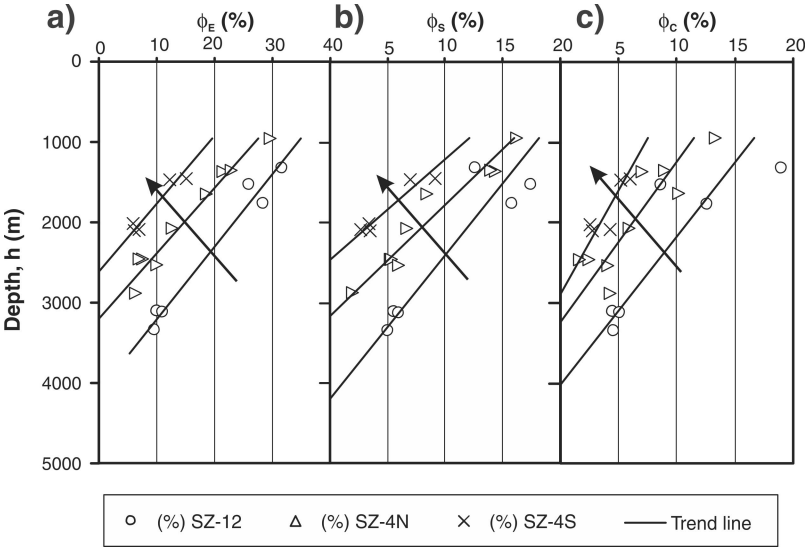

Figure 3. Comparison of the trend lines for the initial stages of the three porosities from the three study zones (SZ), SZ-12, SZ-4N, and SZ-4S (Katsube, et al., 2011). 3a) ϕ_E versus depth, 3b) ϕ_S versus depth and 3c) ϕ_C versus depth. The arrow shows the direction toward the zone of higher compaction rate. SZ-12 represents CZ-1 and CZ-2, SZ-4N represents the southern section of CZ-3 and the northern section of CZ-4 and SZ-4S represent the southern section of CZ-4.

Table 1. Porosity and grain-size data for the 27 shale samples used in this study.

CZ, Well Name & (Number)	Sample	Depth (h)	Tclay (%)	Tsilt (%)	Tsand (%)	ϕ_E	ϕ_S	ϕ_C	SZ
4 Reindeer (D-27)	RE-1	1458	28.934	15.11	5.977	15.1	9.1	6	SZ-4S
	RE-2	1469	31.881	12.3	5.802	12.2	7	5.2	SZ-4S
	RE-3	2022	30.585	13.59	5.854	5.9	3.4	2.5	SZ-4S
	RE-4	2092	25.354	13.48	11.17	7	2.7	4.3	SZ-4S
	RE-5	2099	32.941	13.79	3.283	6.2	3.5	2.7	SZ-4S
	RE-6*	2213	35.318	12.96	1.726	6.6	3.6	3	SZ-4S
	RE-7*	2389	28.742	11.5	9.744	8.7	4.6	4.1	SZ-4S
	RE-8*	2421	19.442	12.34	18.22	7.9	4.2	3.7	SZ-4S
	RE-9*	2551	42.374	7.645	0.0003	8.9	5.1	3.8	SZ-4S
	RE-10*	2725	37.373	11.91	0.743	9.3	5.1	4.2	SZ-4S
	RE-11*	2923	20.745	8.29	20.97	8.5	4.7	3.8	SZ-4S
	RE-12*	3153	18.587	9.46	21.94	6.7	4.1	2.6	SZ-4S
	RE-13*	3481	16.535	9.51	23.99	5.6	2.6	3	SZ-4S
	RE-14*	3628	14.658	7.91	27.45	7	4	3	SZ-4S
1 Nerlerk (J-67)	NR-1*	3658	31.888	14.26	3.844	15.9	7.1	8.8	SZ-12
	NR-2*	3673	44.464	5.52	0.002	16.2	7.6	8.6	SZ-12
	NR-3*	4006	32.375	12.99	4.631	14	8.3	5.7	SZ-12
4 Mallik (A-06)	ML-1	1362	31.995	12.69	5.342	21.4	14.4	7	SZ-4N
	ML-2*	3176	21.028	12.85	16.14	5	3.2	1.8	SZ-4N
	ML-3*	3547	17.963	9	23.05	5.8	3.3	2.5	SZ-4N
2 Amerk (O-09)	AR-3	1765	32.709	12.99	4.316	28.2	15.7	12.5	SZ-12
	AR-7*	4861	40.909	8.73	0.373	8.2	4.8	3.4	SZ-12
3 Taglu (G-33)	TG-1	952	34.372	14.14	1.493	29.5	16.2	13.3	SZ-4N
	TG-3	1640	43.776	6.21	0.041	18.6	8.4	10.2	SZ-4N
	TG-6	2460	48.64	1.35	0	6.9	5.3	1.6	SZ-4N
	TG-7	2533	36.37	12.88	0.765	10	5.9	4.1	SZ-4N
2 Amauligak (F-24)	AM-2	3119	29.481	14.84	5.681	10.8	5.8	5	SZ-12

Tclay: Total clay content
Tsilt: Total silt content
Tsand: Total sand content

ϕ_E: Effective Porosity
ϕ_S: Storage porosity
ϕ_C: Connecting porosity

CZ: Compaction zone
SZ: Study zone

The porosity data are selected from previous publications, ϕ_E from Katsube and Issler (1993), ϕ_S and ϕ_C from Connell-Madore and Katsube (2006). The samples marked with an asterisk are from over-pressured formations. All other samples are from normally pressured formations. The depth (h) values are the true vertical depth values (Katsube and Issler, 1993).

zone with the lowest compaction rate, and the compaction rates increase as the CZ numbers increase. The estimated Pliocene-Pleistocene sedimentation rates for CZ-1 (wells Nerlerk J-67 and Amerk E-90), CZ-2 (wells Amauligak F-24 and Amerk O-09) and CZ-3 (wells Taglu G-33, Taglu C-42 and Taglu F-43) are 570 to 1140 m/Ma, 280 to 570 m/Ma, and 50 to 280 m/Ma, respectively. The wells in CZ-4 (wells Mallik A-06 and Reindeer D-27) have substantially eroded successions below the Pliocene-Pleistocene formations (Issler, 1992). Overpressure occurs below 2.3 km (main overpressure zone below 3 km) at Mallik A-06 and below approximately 2 km at Reindeer D-27 (Issler et al., 2002). Further details on the regional stratigraphy can be found in related publications (e.g. Issler, 1992; Issler et al., 2002).

Figure 1 shows examples of the shale sonic porosity (ϕ_G), determined using downhole sonic logs versus depth (h) relationships for four of the nine petroleum exploration wells in the Beaufort-Mackenzie Basin. Figure 1a shows the ϕ_G-h relationship for well Amerk O-09 representing the trend in CZ-1 and CZ-2. Figures 1b and 1c show the ϕ_G-h relationship for wells Taglu G-33 and Mallik A-06, representing the trends in CZ-3 and the northern part of CZ-4, respectively. Figure 1d shows the ϕ_G-h relationship for the Reindeer D-27 well, representing the trend in the southern section of CZ-4. Figure 1 shows that compaction gradients (CG) in the normally pressured zone (2–4 km depth) increase from approximately 0.9%/100 m in CZ-2 to nearly 1.2%/100 m in CZ-4. The CG is represented by the sonic porosity % decrease per 100 m depth (ϕ_G%/100 m). Although these differences are relatively small, they are consistent with the larger data set of Issler (1992) that shows an increase in CG with declining sedimentation rates from offshore to onshore regions. The larger CG values represent larger ϕ_G decreases increased depth.

METHOD OF INVESTIGATION

Connell-Madore and Katsube (2006) used the published ϕ_E values of Katsube and Issler (1993) and the corresponding mercury intrusion and extrusion data obtained at the time of these measurements to determine the ϕ_S and ϕ_C values of the 27 shale samples used in this study. These 27 samples are from six of the nine wells that were previously used to collect the 41 shale samples used for the pore-size distribution measurements (Katsube and Issler, 1993).

Details of the mercury porosimetry method and the procedures for obtaining the three porosities (ϕ_E, ϕ_S, ϕ_C) are described in Katsube (2000) and Connell-Madore and Katsube (2006) (Fig. 4, 5). By this method mercury is forced into a shale sample under pressure, and the total volume of mercury intruded is used to determine the effective porosity (ϕ_E). The total amount of mercury that extrudes from the sample after the pressure is released (Fig. 6) is used to determine the connecting porosity (ϕ_C) (Wardlaw and Taylor, 1976). The storage porosity (ϕ_S) is represented by the amount of mercury trapped in the sample after the pressure is released. Its value is determined by the difference between ϕ_E and ϕ_C. The ϕ_S represents mainly the intergranular pore space and ϕ_C represents mainly the interconnected pore space between the storage pores (Fig. 4) which provides the main pathway for fluid migration in these shales. The ϕ_E is the sum of these two porosities, but is not the total porosity (ϕ_T) of a rock, because it does not include the pore space of isolated pores. According to a previous study (Bowers and Katsube, 2002), ϕ_C is more sensitive to overpressure than ϕ_S in deep formations. The grain-size analysis data used in this study were performed by the AGAT Laboratories (Calgary, Alberta).

In this study, we adopt the sample grouping system adopted by a previous study (Katsube, et al., 2011), where the compaction zones (CZ) of 41 shale samples were grouped into three study zones (SZ), SZ-12, SZ-4N and SZ-4S, in order of lower to higher compaction gradient (CG = ϕ_G%/100 m). There were only five samples from CZ-1 and they were from near the bottom of wells Arluk E-90 and Nerlerk J-67 (Fig. 2, Table 1). Therefore, they were lumped together with the ten samples from CZ-2 that cover a broader depth range (wells Amauligak F-24 and Amerk O-09) to form SZ-12. SZ-4N consists of 12 samples from four wells (Mallik A-06, Taglu F-43, Taglu G-33 and Taglu C-42) close to the boundary between CZ-3 and CZ-4 (Fig. 2, Table 1). Fourteen samples from the Reindeer D-27 well in the southern part of CZ-4 are included in SZ-4S (Fig. 2, Table 1). This implies that SZ-4S simulates the zone with highest compaction rate and lowest Pliocene-Pleistocene sedimentation rate,

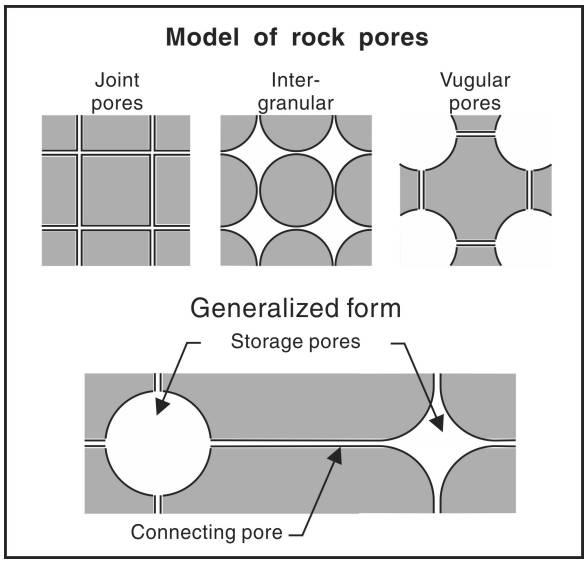

Figure 4. Storage and connecting-pore model used for characterizing shales (Katsube and Williamson, 1994, 1998). The storage pores represent the storage porosity (ϕ_S) and the connecting pores represent the connecting porosity (ϕ_C) which provides the pathway for fluid migration in these shales. Joint pores are usually referred to as connecting pores, and intergranular and vugular pores are the two types of storage pores.

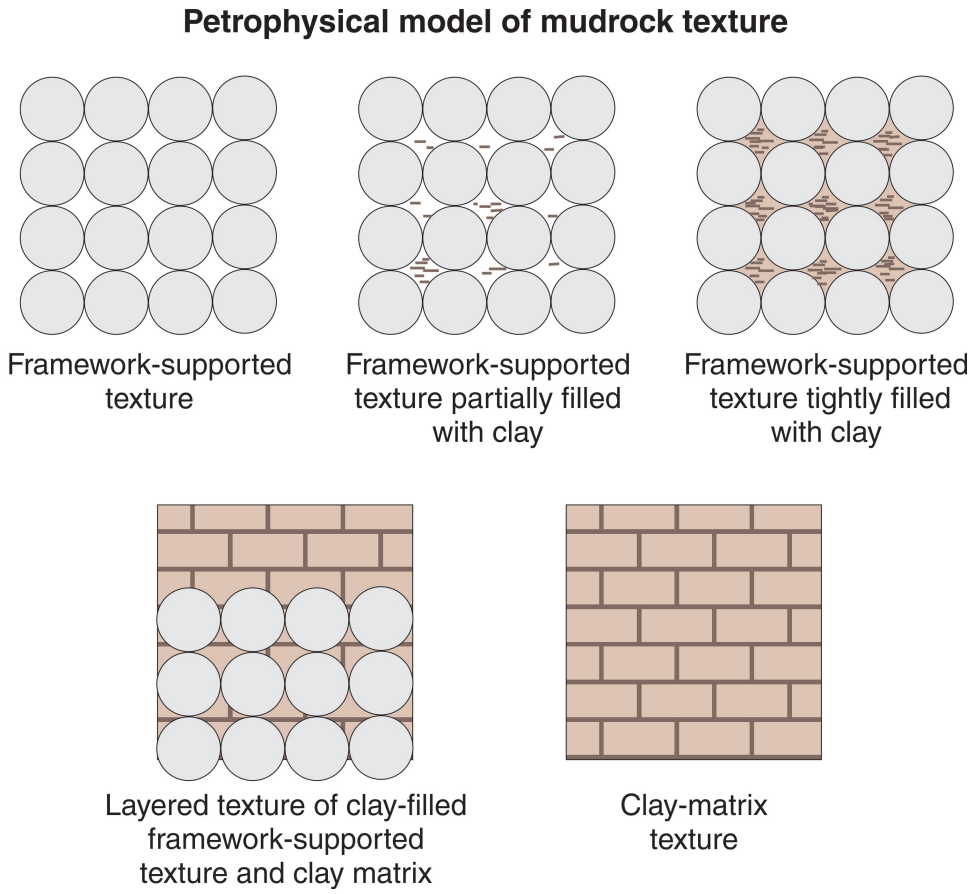

Figure 5. Pore structure consisting of different grain sizes, represented by sand and clay grains (Katsube et al., 2006).

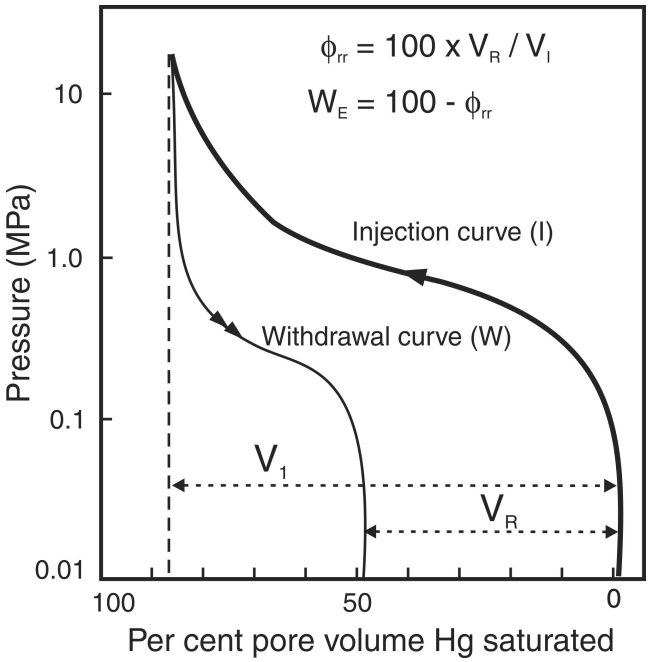

Figure 6. Diagram (*modified from* Wardlaw and Taylor (1976)) describing the mercury intrusion and extrusion curves and explaining the definitions and methods for determining withdrawal efficiency (W_E) and storage porosity ratio ($\phi_{rr} = \phi_S/\phi_E$). V_I and V_R are the total mercury intrusion volume and total residual volume, respectively.

SZ-4N simulates the zone with the intermediate compaction rate and intermediate Pliocene-Pleistocene sedimentation rate, and SZ-12 simulates the zone with the lowest compaction rate and highest Pliocene-Pleistocene sedimentation rate. When considering the locations of these study-zones in Figure 2, it can be considered that the compaction rates increase from the offshore location, represented by SZ-12, toward the onshore location represented by SZ-4S.

EXPERIMENTAL RESULTS

The results of the grain-size analysis performed by the AGAT Laboratory (Calgary, Alberta) and the published results of the three porosities (ϕ_E, ϕ_S, ϕ_C) (Connell-Madore and Katsube, 2006) for the 27 shale samples from six of the nine wells (Fig. 2) are listed in Table 1. The four compaction zones (CZ) consisting of the Cretaceous and Paleogene sediments located under the Pliocene-Pleistocene formations with the different sedimentation rates and the three study zones (SZ), SZ-12, SZ-4N and SZ-4S, for which the wells are located, are all listed in that table. The depth (h) in this table represents the true vertical depth (Katsube and Issler, 1993).

The porosity-versus-depth relationships of the three porosities (ϕ_E, ϕ_S, ϕ_C) are displayed in Figure 7 for the three study zones. The porosity-versus-depth relationships of the three porosities with their trend lines and the total sand (Tsand), total silt (Tsilt) and total clay (Tclay) values versus depth relationships with their trend lines are displayed in Figure 8 for SZ-12, in Figure 9 for SZ-4N, and in Figure 10 for SZ-4S. The comparison among the porosity versus depth with their trend lines for the three study zones are shown in Figure 11a. The comparison between the three grain sizes (Tsand, Tsilt, Tclay) versus depth with their trend lines are shown in Figure-11b. The trend line function and the R-square (R^2) values of Excel were used to fit the data in these figures.

DATA ANALYSIS

The three porosities (ϕ_E, ϕ_S, ϕ_C) versus depth (h) for the three study zones (SZ-12, SZ-4N and SZ-4S) are shown in Figure 3 and 11a as previously indicated. The relationships between the trend lines of the three porosities versus depth (ϕ_E/h, ϕ_S/h, ϕ_C/h) and those of the three grain sizes versus depth (Tsand/h, Tsilt/h and Tclay/h) are shown in Figures 8, 9 and 10. Most of the porosity trend lines show good representations of their data with R-square (coefficient of determination: R^2) values above 0.7, but all of the grain size trend lines do not show good representation of their data, displaying low R^2 values. Nonetheless, the relationships between the two trend line sets have been used for the porosity versus grain-size analysis in this study. Following are these results of the porosity versus grain-size relationship analysis for each of the study zones.

SZ-12

We suggest that each of the ϕ/h relationships for the three porosities of SZ-12 shown in Figure 8a can be represented by single trend lines, although they are a mixture of normal and over-pressure data points. The total sand versus depth (Tsand/h), total silt versus depth (Tsilt/h), and total clay versus depth (Tclay/h), plots with their trend lines for the same study zone are shown in Figure 8b.

The ϕ_E values (Fig. 8a1) show a significant decrease with increased depth. This trend cannot be explained by the Tsand (Fig. 8b1) decrease with increased depth, because its decrease is very minor (<5%) compared to the ϕ_E decrease which is about 20% for the same depth range. The Tsilt decrease (Fig. 8b2) with increased depth, in this case, is likely to open up intergranular pore space between the sand grains and increase the ϕ_E value, so it does not contribute to the ϕ_E decrease. The slight Tclay increase with increased depth (Fig. 8b3) is likely to have some contribution in the ϕ_E decrease, although its increase (about 10%) is likely to be too small to be a significant factor. Although there are clearly some factors that are contributing to the ϕ_E decrease in this case, it has to be concluded that their effects are too small and that increased confining pressure has to be considered the main factor for the ϕ_E decrease (Fig. 9a1).

SZ-4N

The relationships of the three porosities for the normal pressure sections of SZ-4N are shown in Figure 9a with their trend-lines, but with the two over-pressure porosity data points treated separately. The three grain sizes versus depth (Tsand/h, Tsilt/h and Tclay/h) data points with their trend lines for the same ϕ/h points, as above, are shown in Figure 9b.

The ϕ_E for the normal pressures show a significant decrease (Fig. 9a1) with increased depth, but this trend cannot be explained by the very slight Tsand (Fig. 9b1) decrease with increased depth. The Tsilt (Fig. 9b2) decrease with depth cannot explain the ϕ_E decrease either, because its decrease is more likely to open up intergranular pore space in the sand and increase the ϕ_E values. The Tclay's approximately 5 to 20% increase with depth shown in Figure 9b3 will certainly be a contribution to the ϕ_E decrease with depth, but it is questionable if it will be enough for the over 20% ϕ_E decrease with depth seen in Figure 9a1, for the 1000 to 3000 m depth range. This is because the R^2 value of the Tclay is very low (<0.31). This suggests that increased confining pressure with increased depth has to be considered the main cause of the decrease. However, a very different analysis of these data is also possible. For example, if the Tsilt data point at 2533 m depth in Figure 9b2 is ignored, the four Tsilt data points above that depth can represent a significant Tsilt decreasing rate with depth that could help explain the rapid ϕ_E decreasing rate in Figure 9a1, since the Tsand decreasing rate in Figure 9b1 is insignificant and Tsilt could be the main source

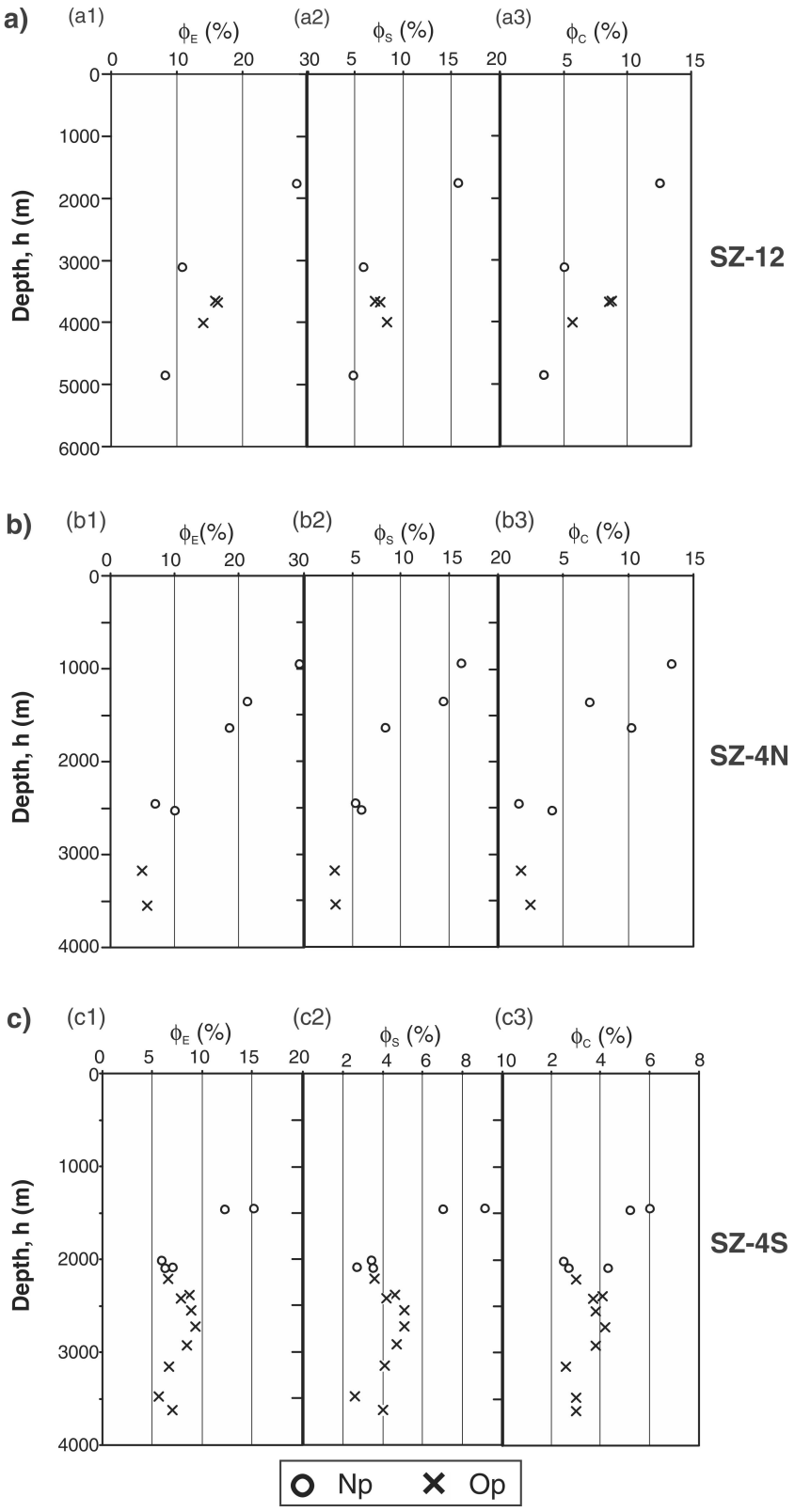

Figure 7. Porosity versus depth (h) relationships for the three porosities (ϕ_E, ϕ_S, ϕ_C) in the three study zones (SZ): **a)** SZ-12, b) SZ-4N, and c) SZ-4S. Np: normal pressure, Op: over pressure.

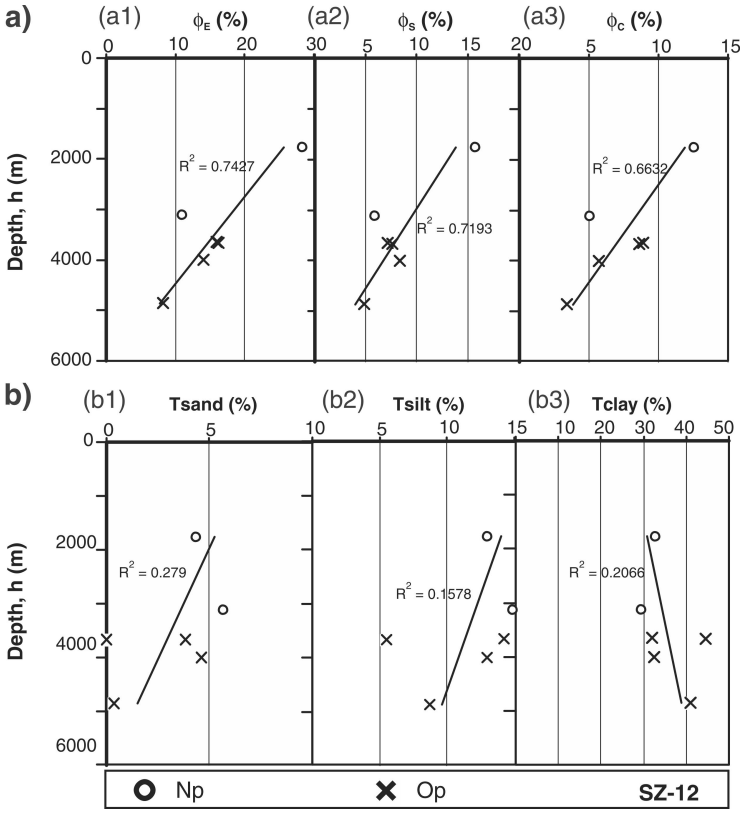

Figure 8. The porosity-versus-depth (h) relationships **a)** for the three porosities (ϕ_E, ϕ_S, ϕ_C) with their trend lines, and **b)** for the three grain-size contents (Tsand, Tsilt, Tclay) with their trend lines, in SZ-12. Np: normal pressure, Op: over pressure. R^2: coefficient of determination.

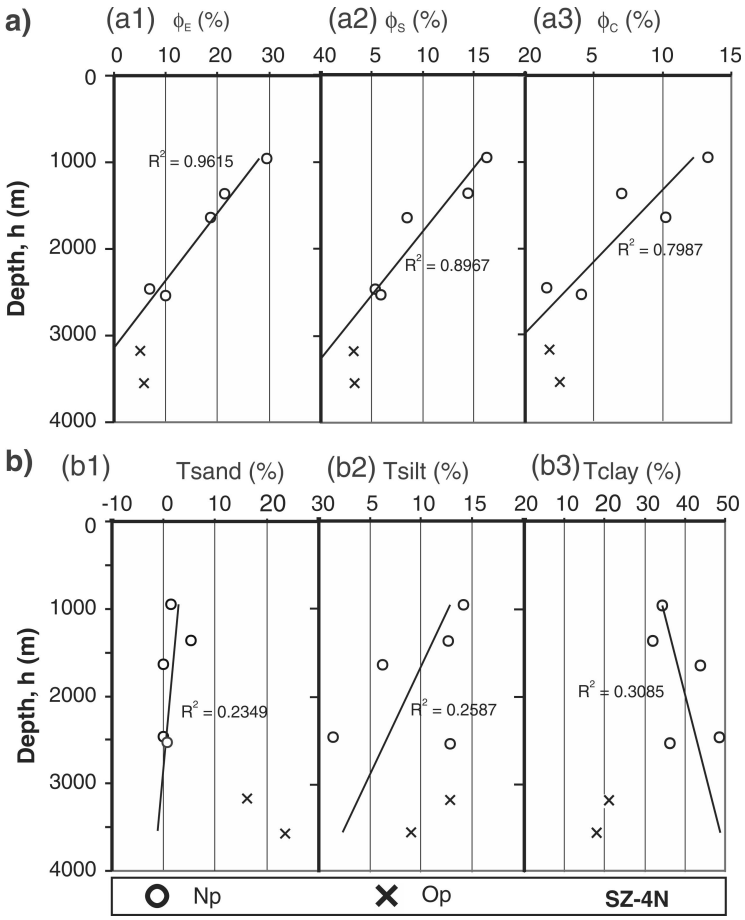

Figure 9. The porosity-versus-depth (h) relationships **a)** for the three porosities (ϕ_E, ϕ_S, ϕ_C) with their trend lines, and **b)** for the three grain-size contents (Tsand, Tsilt, Tclay) with their trend lines, in SZ-4N. Np: normal pressure, Op: over pressure. R^2: coefficient of determination.

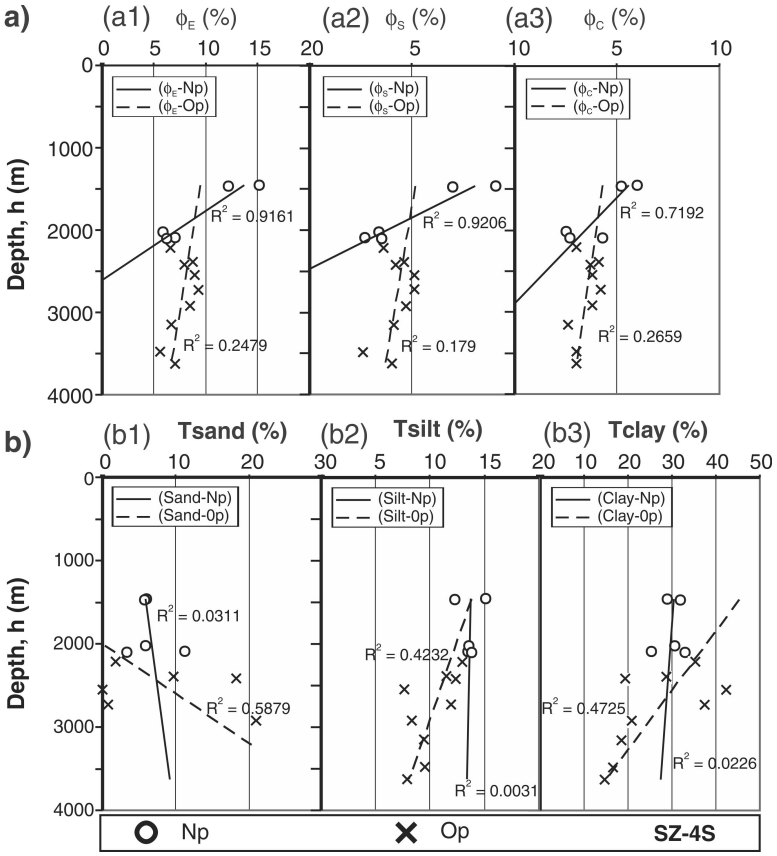

Figure 10. The porosity-versus-depth (h) relationships **a)** for the three porosities (ϕ_E, ϕ_S, ϕ_C with their trend lines, and **b)** for the three grain-size contents (Tsand, Tsilt, Tclay) with their trend lines, in SZ-4S. Np: normal pressure, Op: over pressure. R^2: coefficient of determination.

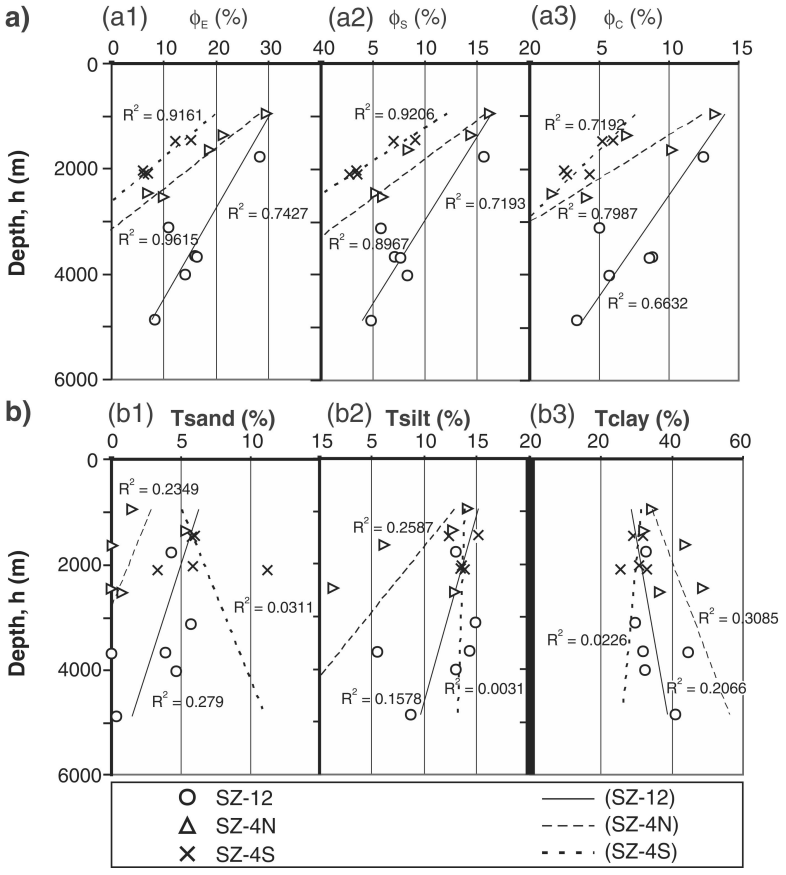

Figure 11. Comparison of the trend lines for **a)** initial stages of the three porosities from the three study zones (SZ-12, SZ-4N, and SZ-4S) (Katsube, et al., 2011), and **b)** three grain-sizes (Tsand, Tsilt, Tclay) from the same study zones. R^2: coefficient of determination.

of the ϕ_E. Although, this Tsilt decrease (Fig. 9b2) and Tclay increase (Fig. 9b3) are definitely a possible contribution to the ϕ_E decrease, it is not certain that they are the only causes of the ϕ_E decrease, so that a possible contribution from the increased compaction cannot be ignored.

The two relatively low over-pressured porosity data points in Figures 9a1 to 9a3 cannot be explained by the slightly high Tsand (Fig. 9b1) and low Tclay values in Figure 9b3. It is likely that the high Tsilt values in Figure 9b2 have some effect in reducing the ϕ_E by blocking the intergranular pores of the sand, but with the low Tclay content, it is most likely that increased confining pressure with increased depth is the main contribution in lowering the ϕ_E of these low over-pressured porosity values.

SZ-4S

The ϕ/h relationships for the three porosities of SZ-4S are shown in Figure 10a combined with both the normal and over-pressured data points with their trend-lines.

The porosities for the normal-pressure data generally represent the initial stage of the compaction to a depth of just over 2000 m. The porosity decrease with increased depth from about 1500 to 2000 m is about 10% for ϕ_E (Fig. 10a1), but is slightly less for ϕ_S (Fig. 10a2) and considerably less for ϕ_C (Fig. 10a3). The slight increasing trend for Tsand trend lines (Fig. 10b1), the slight decreasing trend for Tsilt trend lines (Fig. 10b2), and the almost no change for the Tclay trend lines (Fig. 9b3) do not explain the decreases for the three porosities in Figures 10a1, 10a2, and 10a3. This suggests that increased confining pressure with increased depth has to be the only cause for the decrease of the three normal-pressure porosities with increased depth.

The rapid increasing trend for Tsand trend lines (Fig. 10b1), the moderate decreasing trend for Tsilt trend lines (Fig. 10b2), and the rapid decreasing trend for Tclay trend lines (Fig. 10b3) above the 2000 m depth do not explain the general slight decreasing trends for trend lines for the three over-pressured porosities in Figures 10a1, 10a2, or 10a3. The rapid trend-line increase for Tsand (Fig. 10b1) may explain the partial increase for the five over-pressured porosity data points for the depth range of 2200 to 2700 m (Fig. 10a1, 10a2, and 10a3). However, their general decrease with depth of the three over-pressured porosities for the entire depth range is most likely the result of increased confining pressure due to increased depth.

Porosity characteristic variations of the three study zones

All three porosities (ϕ_E, ϕ_S, ϕ_C) decrease with increased depth mainly for the initial depth sections of all three study zones, as shown in Figure 3 and in Figure 11a. Only the data for SZ-12 include the overpressured data points. The shale-sample porosities from the lower compaction zones with higher sedimentation rates have generally higher porosities than those from the higher compaction zones with lower sedimentation rates, as shown in Figure 11a1, 11a2, and 11a3. The texture data for these shale samples are shown in Figure 11b. In Figures 11b1, 11b2, and 11b3 are shown the Tsand, Tsilt, and Tclay versus depth values with their trend lines for the same porosity data points in Figure 11a. However, these grain-size trend lines in Figure 11b do not necessarily support the ϕ_E trend lines in Figure 11a. For example, although the directions of the Tsand trend lines for study zones SZ-12 and SZ-4N in Figure 11b1 are somewhat similar to those for the ϕ_E variation in Figure 11a1, their degree of variation is too small to support the ϕ_E value variations in Figure 11a1. In addition, the direction of the trend line for SZ-4S in Figure 11b1 is opposite to that of ϕ_E in Figure 11a1 for the same study zone. The relationship between the ϕ_S (Fig. 11b2) and Tsand (Fig. 11a2) are somewhat similar to those for ϕ_E (Fig. 11b1) and Tsand (Fig. 11a1). Although the increasing direction of the Tclay trend-lines in Figure 11b3 for SZ-12 and SZ-4N support the decreasing trends of ϕ_E in Figure 11a1 to a certain extent, as previously indicated, the Tclay trend line for SZ-4S does not. In addition, the range of the Tclay value variations are generally different from those in any of the three figures in Figure11a. As a result, although there may be some cases that the texture supports the ϕ_E trends, they are minor and almost irrelevant. Therefore, in conclusion, the texture characteristics for these shale samples do not provide a comprehensive explanation for any of the differences between the porosity characteristics of the three study zones. This implies that these porosity characteristic differences must be representing compaction pressure differences between the three study zones.

CONCLUSIONS

The results of this study show that all three porosities (ϕ_E, ϕ_S, ϕ_C) decrease with increased depth, in mainly the initial depth sections, for all three study zones: SZ-12, SZ-4N, and SZ-4S. However, the total sand (Tsand), total silt (Tsilt), and total clay (Tclay) versus depth data generally do not consistently support the porosity decrease with the increased depth relationships. There is a case where the Tsand decreases with increased depth and does supports the ϕ_E decrease to a certain extent, but its decrease is too small to provide a full explanation for the total ϕ_E decrease. Also there are some cases where Tclay increases with increased depth and clearly supports the ϕ_E decrease, but not to an extent to fully support the entire ϕ_E decrease rate. There is one case where the Tclay increase does support the ϕ_S decrease with depth, but such cases are not consistent. Apart from these specific cases, it has to be concluded that changes in the shale texture characteristics do not generally explain the porosity-versus-depth characteristics of these shale samples, and that increased compaction pressure with increased depth has to be the main cause of the general decrease of the three porosities.

All three porosities decrease with increased depth in all three study zones, as previously indicated. However, the porosity values for the shale samples from the study zones with the lower compaction and higher sedimentation rates (e.g. SZ-12) show generally higher values than those from the study zones with higher compaction and lower sedimentation rates (e.g. SZ-4S). Differences in the shale texture that consistently support these porosity differences have not been found in this study. Therefore, as a conclusion, compaction pressure differences in the study zones are considered to be the main source of the differences in the general porosity values. Since these study zones represent the compaction zones in Figure 2, this study concludes that the lower compaction zones with higher sedimentation rates have generally higher porosities which decrease as these zones move from the offshore regions toward the zones of higher compaction and lower sedimentation rates at the onshore region of the Beaufort-Mackenzie Basin.

The results of this study are expected to provide information that can be used to improve the interpretation of geophysical methods when evaluating shale-seal characteristics related to hydrocarbon fluid and gas leakage possibilities (Katsube et al., 2006), possible existence of overpressure which can be a source of blowouts during offshore drilling, and other characteristics necessary for hydrocarbon exploration.

ACKNOWLEDGMENTS

The authors express their gratitude to Barbara Medioli (GSC Ottawa) for critically reviewing this paper and for her very constructive and useful suggestions. The authors also thank Dr. D. Issler (GSC Calgary) for his advice on the format of this paper and for his suggested title for this paper. The authors express their gratitude to the AGAT Laboratories (Calgary, Alberta) for performing the grain-size analysis of the 27 shale samples used in this study.

REFERENCES

Bowers, G.L., 1995**.** Pore pressure estimation from velocity data: accounting for overpressure mechanisms besides undercompaction; Society of Petroleum Engineers Drilling and Completion, v. 10, no. 2, p. 89–95.

Bowers, G.L. and Katsube, T.J., 2002**.** The role of shale pore-structure on the sensitivity of wireline logs to overpressure; *in* Pressure regimes in sedimentary basins and their prediction, (ed.) A.R. Huffman and G.L. Bowers; American Association of Petroleum Geologists, Memoir 76, p. 43–60.

Connell-Madore, S. and Katsube, T.J., 2006**.** Pore-size distribution characteristics of Beaufort-Mackenzie Basin shale samples; Geological Survey of Canada, Current Research 2006-B1, 13 p. doi:10.4095/222398

Issler, D.R., 1992. A new approach to shale compaction and stratigraphic restoration, Beaufort-Mackenzie Basin and Mackenzie Corridor, Northern Canada; AAPG Bulletin, v. 76, p. 1170–1189.

Issler, D.R. and Katsube, T.J., 1994**.** Effective porosity of shale samples from the Beaufort-MacKenzie Basin; *in* Current Research, Part B, Geological Survey of Canada, Paper 94–1B, p. 19–26.

Issler, D.R., Katsube, T.J., Bloch, J.D., and McNeil, D.H., 2002. Shale compaction and overpressure in the Beaufort-Mackenzie Basin of northern Canada; Geological Survey of Canada, Open File 4192, 1 CD-ROM. doi:10.4095/213052

Huffman, A.R., and Bowers, G.L., 2002**.** Pressure regimes in sedimentary basins and their prediction, American Association of Petroleum Geologists, Memoir 76, 238 p.

Katsube, T.J., 2000**.** Shale permeability and pore-structure evolution characteristics; implications for overpressure; Geological Survey of Canada, Current Research 2000-E15, 9 p. doi:10.4095/211622

Katsube, T.J., Issler, D.R., and Connell-Madore, S., 2006. Storage and connecting pore structure of mudstone-shale and its effect on seal quality: tight shales that may leak; *in* Abstract Volume, American Association of Petroleum Geologists, International Conference and Exhibition, November 5–8, 2006, Perth Australia, p. 60.

Katsube, T.J. and Issler, D.R., 1993**,** Pore-size distributions of shales from the Beaufort-Mackenzie Basin, northern Canada; *in* Geological Survey of Canada, Current Research, 93–1E, p. 123–132.

Katsube, T.J. and Williamson, M.A., 1994**,** Shale petrophysics and basin charge modelling; *in* Current Research, Part D, Geological Survey of Canada, Paper 94–1D, p. 179–188.

Katsube, T.J. and Williamson, M.A., 1998**,** Shale petrophysical characteristics: permeability history of subsiding shales; *in* Shales And Mudstones II : Petrography, Petrophysics, Geochemistry and Economic Geology, (ed.) J. Schiber, W. Zimmerle, and P.S. Sethi; E. Schweizerbart Science Publishers, Stuttgard, p 69–91.

Katsube, T.J., Issler, D.R., and Connell-Madore, S., 2011**,** Porosity characteristics of shale samples for varied compaction zones in the Beaufort-Mackenzie Basin, Northwest Territories; Geological Survey of Canada, Current Research 2011-12, 14 p. doi:10.4095/289040

Wardlaw, N.C. and Taylor, R.P., 1976. Mercury capillary pressure curves and the interpretation of pore structure and capillary behaviour rocks; Bulletin of Canadian Petroleum Geology, v. 24, p. 225–262.

Youn, S.H., 1974**,** Comparison of porosity and density values of shale from cores and well logs: Master's thesis, University of Tulsa, Tulsa, Oklahoma, 62 p.

Geological Survey of Canada Project EGM003